

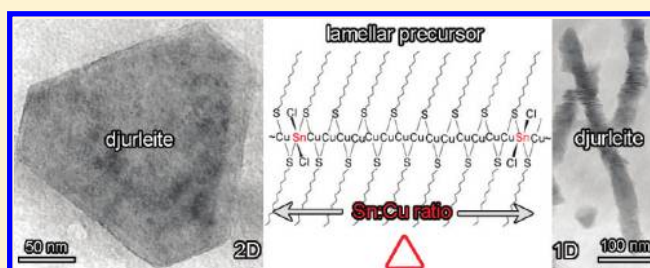
From Ultrathin Two-Dimensional Djurleite Nanosheets to One-Dimensional Nanorods Comprised of Djurleite Nanoplates: Synthesis, Characterization, and Formation Mechanism

Luoxin Yi and Mingyuan Gao*

Institute of Chemistry, Chinese Academy of Sciences, Bei Yi Jie 2, Zhong Guan Cun, Beijing 100190, China

S Supporting Information

ABSTRACT: Sn-doped ultrathin copper sulfide nanosheets of 209 ± 33 nm and nanoplates of 36.0 ± 5.9 nm were synthesized by pyrolyzing copper(II) acetylacetonate ($\text{Cu}(\text{acac})_2$) in dodecanethiol in the presence of different amounts of $\text{SnCl}_4 \cdot 5\text{H}_2\text{O}$. The large nanosheets appeared in hexagonal and quasi-triangular shapes, while the small nanoplates presented mainly triangular shapes. Transmission electron microscopy (TEM) studies revealed that both nanosheets and nanoplates tended to form face-to-face stacking, which was further confirmed by X-ray diffraction studies. Such a self-assembling tendency became so strong for the small nanoplates that they formed one-dimensional (1D) self-assembled nanorods of 365 ± 145 nm. Atomic force microscopy studies revealed that the thickness of nanosheets was around $6.4\text{--}6.6$ Å. The powder X-ray diffraction and high resolution TEM investigations demonstrated that the resultant two-dimensional (2D) nanocrystals are of monoclinic djurleite (Cu_3S_{16}). Further investigations on different control samples revealed that Sn could partly replace Cu in forming lamellar supramolecular structures which actually acted as the precursors for the ultrathin 2D djurleite nanocrystals. Because of the excellent thermal stability and protective effects, the Sn-dodecanethiol complexes survived the pyrolysis of $\text{Cu}(\text{acac})_2$ and preferentially attached on $\{100\}$ facets of the resultant djurleite nanocrystals. Consequently, the growth of djurleite nanocrystals along the $[100]$ direction was blocked, resulting in 2D Cu_3S_{16} nanocrystals. The dipole–dipole interaction along the $[100]$ direction and the hydrophobic interaction between the nanoplates were the main driving force for the formation of 1D superstructures of the nanoplates.



INTRODUCTION

Two-dimensional (2D) nanomaterials such as nanosheets and nanoplates are especially worth researching because they as building blocks are superior over spherical nanocrystals for constructing nanodevices with desired crystal orientation owing to their anisotropic structures.^{1–5} In particular, recent developments on 2D crystalline nanosheets such as graphene⁶ and transition-metal chalcogenides^{7–9} have sparked tremendous research interest for exploring the synthesis and physical properties of 2D nanomaterials as they are potentially useful not only for developing new generation of optoelectronic devices,¹⁰ but also for high performance catalysts.¹¹

Anisotropic bulk materials such as inorganic layered materials are the most effective precursors for achieving 2D nanomaterials. As a matter of fact, many inorganic layered materials exist possessing strong in-plane bonds and weak van der Waals-like coupling between layers. Owing to such a layered structure, they can be split into individual atomic layers through chemical exfoliation^{12,13} or mechanical exfoliation methods by which nanosheets such as BN,^{14,15} BiTe,⁸ MoS₂,⁹ WS₂,⁹ MoSe₂,⁹ and graphene⁶ have been obtained, and the thickness of the resultant

2D materials is often composed of a few atomic layers. Apart from the inorganic layered materials, metal–organic layered solids were also found to be able to be transformed into 2D inorganic nanomaterials under proper chemical reactions.^{16–18} For example, layered $\text{AgSC}_{12}\text{H}_{25}$ was used as a precursor to prepare uniform Ag nanodisks by the solventless thermolysis method.¹⁹ In a similar way, amorphous Bi nanofilms with a thickness of several atoms (0.6 nm) and uniform Cu_2S nanodisks of 10 nm thick were successfully obtained via the solventless thermolysis of layered $\text{Bi}(\text{SC}_{12}\text{H}_{25})_3$ and layered $\text{Cu}(\text{SC}_{12}\text{H}_{25})_2$, respectively.^{20,21} In-depth studies on the formation mechanism of 2D nanomaterials via the thermolysis of metal–organic layered precursors suggest that the growth of these 2D nanocrystals is achieved largely due to the constraint from the layered structure of the precursors.²¹

Although various types of solution-based synthetic approaches are widely utilized for synthesizing semiconductor, metal, and

Received: October 8, 2010

Revised: December 31, 2010

metal oxide nanocrystals with various morphologies and well-defined nanostructures, they remain less successful in achieving 2D nanomaterials in comparison with their zero-dimensional (0D) and one-dimensional (1D) counterparts.^{22–24} With respect to the formation of 2D nanostructures, preferential growth along two axes has to be promoted with the growth along the third axis being blocked.^{25,26} So far, only a few 2D nanomaterials have been synthesized, such as metallic cobalt nanodiscs²⁷ and lanthanide oxide nanoplates^{28,29} upon the solution-based synthetic methods.

Nanocrystals of metal sulfides have driven particularly extensive investigations among all types of inorganic nanocrystals in recent years.^{30–41} Metal sulfides have narrow band gaps and band edge levels at relatively negative potentials compared with their corresponding oxides. Thus, the metal sulfides could be good candidates for solar energy cells, photocatalysts, and water treatment.^{42–52} For instance, Cu_{2-x}S is a *p*-type semiconductor with an *x*-dependent band gap energy varying from ~ 1.2 eV for chalcocite ($x = 0$) to ~ 1.5 eV for digenite ($x = 0.2$), accompanied by a transformation from an indirect band gap semiconductor into a direct band gap one. Djurleite is a copper sulfide mineral with a formula of $\text{Cu}_{31}\text{S}_{16}$. In the crystal structure, djurleite has a monoclinic structure with a large unit cell containing 248 copper and 128 sulfur atoms.⁵³ Our previous studies have shown that $\text{Cu}_{31}\text{S}_{16}$ nanocrystals can be used as a seed catalyst to assist the heterogrowth of other types metal sulfide nanomaterials.^{54,55} It has also been demonstrated that by pyrolyzing copper(II) acetylacetonate ($\text{Cu}(\text{acac})_2$) in dodecanethiol at 200 °C, uniformly sized $\text{Cu}_{31}\text{S}_{16}$ nanocrystals can easily be produced.⁵⁴ Following from our previous investigations, we herein report djurleite nanosheets and 1D nanorods formed upon the self-assembly of djurleite nanoplates which were prepared by pyrolyzing $\text{Cu}(\text{acac})_2$ in dodecanethiol in the presence of SnCl_4 . The mechanisms for the formation of ultrathin djurleite nanosheets and 1D self-assembled structure made up of djurleite nanoplates are discussed.

EXPERIMENTAL SECTION

Chemicals. Stannic chloride pentahydrate ($\text{SnCl}_4 \cdot 5\text{H}_2\text{O}$, 99%) and copper(II) acetylacetonate ($\text{Cu}(\text{acac})_2$, 97%) were purchased from Shanghai Jingchun Chemical Company; *n*-dodecanethiol (98%) was obtained from Shanghai Chemical Company. Other solvents such as ethanol and dichloromethane were analytical grade and used as received.

Synthesis of Djurleite Nanosheets. Typically, 0.262 g (1.00 mmol) of $\text{Cu}(\text{acac})_2$ and 0.175 g (0.50 mmol) of $\text{SnCl}_4 \cdot 5\text{H}_2\text{O}$ (molar ratio of Cu to Sn is 2:1) were first dissolved into 30 mL of *n*-dodecanethiol under magnetic stirring, and then nitrogen gas was introduced to purge the reaction solution. After ~ 20 min, the flask containing the sky-blue mixture was quickly immersed in an oil bath of 200 °C. With the increase of the reaction temperature (*T*), the reaction mixture changed from turbid blue ($T < 90$ °C) to turbid white ($T > 90$ °C). When *T* reached ~ 130 °C, the reaction mixture abruptly turned transparent yellow, and then to opaque brown when *T* arriving at 200 °C, indicating the formation of nanocrystals. Usually it took approximately 15 min for the temperature of the reaction mixture to increase to 200 °C in the oil bath. The reaction mixture was maintained at 200 °C for 48 min and then cooled down to room temperature. The resultant solution was dripped into 7-fold ethanol (by volume) to precipitate nanocrystals which were subsequently collected by centrifugation at 4000 rpm for 10 min. The following purification procedures included the redispersion of the nanocrystals in dichloromethane (equal volume to the resultant solution) and the collection of the nanocrystals

by centrifugation at 4000 rpm for 10 min. Typically, the redispersion/centrifugation procedures were repeated twice before a final elimination of large agglomerates by centrifugation at 2000 rpm for 5 min. Eventually, the resultant nanocrystals dispersed in dichloromethane were obtained for further characterizations.

In order to follow the growth of the final nanocrystals, two additional intermediate products of the aforementioned reaction were extracted during the preparation. The first one was obtained right after the reaction temperature reached 140 °C, while the second one was obtained after the reaction mixture was maintained at 200 °C for 12 min. The first sample was precipitated from the reaction mixture by 7-fold ethanol. After being washed by ethanol three times, it appeared as a light yellow powder in the dry state and was denoted as I-sample 1 (intermediate sample 1). The second sample, denoted as I-sample 2 was purified according to the procedures described for the final nanocrystal product. I-sample 1 was extracted at 140 °C because according to a previous investigation the C–S bond in $\text{Cu}(\text{SC}_{12}\text{H}_{25})_2$ complex is broken at 142.3 °C.²¹

Synthesis of Djurleite Nanoplates Capable of Forming 1D Self-Assembled Superstructures. To further tune the morphology of the resultant djurleite nanosheets, the Cu to Sn ratio was increased to 8:1 for a new set of preparations with the preparative and sample purifying procedures being kept the same. The resultant djurleite nanosheets were greatly reduced in size and termed as nanoplates below. Moreover they tended to form 1D self-assembled nanorods with a very uniform rod width.

Characterizations. Transmission electron microscopy (TEM) images and selected area electron diffraction (SAED) patterns were recorded on a JEM-100CXII electron microscope operating at an accelerating voltage of 100 kV to show the general morphology of the resultant nanomaterials. High resolution TEM (HRTEM) images were taken on FEI Tecnai 20 working at an accelerating voltage of 200 kV for further showing the lattice structure of the nanocrystals. The morphologies of the metal sulfide nanocrystals were investigated by atomic force microscopy (AFM) using Digital Instruments Nanoscope IIIa Multi-mode System (Santa Barbara, CA). Tapping-mode was adopted to acquire the AFM images with the aid of a silicon cantilever equipped with an E-scanner. The scan speed was 1.3 Hz. No additional image processing was made except for flattening. Powder X-ray diffraction (XRD) was taken with a RigakuD/Max-2500 diffractometer under $\text{Cu-K}\alpha_1$ radiation ($\lambda = 1.54056$ Å) to investigate the crystalline structure of the resultant nanomaterials. The Cu and Sn contents were determined by the inductively coupled plasma optical emission spectrometer (ICP-OES) method using a Thermo Fisher IRIS Intrepid II XSP. X-ray photoelectron spectroscopy (XPS) measurements were performed with an ESCALAB 220i-XL photoelectron spectrometer from VG Scientific using 300 W Mg KR radiation (1253.6 eV) for investigating the binding state of Sn and Cu apart from providing their quantification information in the resultant nanomaterials.

RESULTS

Djurleite Nanosheets. The preparative procedures of the djurleite nanosheets were similar to those for $\text{Cu}_{31}\text{S}_{16}$ nanocrystals reported previously.⁵⁴ The only difference is that in the current reaction system $\text{SnCl}_4 \cdot 5\text{H}_2\text{O}$ was introduced. The nanocrystals obtained by Cu to Sn ratio of 2:1 are shown in Figure 1. In general, the resultant nanosheets present quasi-triangular and hexagonal structures with an opposite side distance of 209 ± 33 nm. Moreover, they tend to stack onto each other forming aggregates composed of several pieces of the nanosheets. Under high resolution TEM operating at 200 kV, as shown in Figure 1b, the nanosheets remain quite stable. In spite of the heavy stacking, a single piece of nanosheets appearing

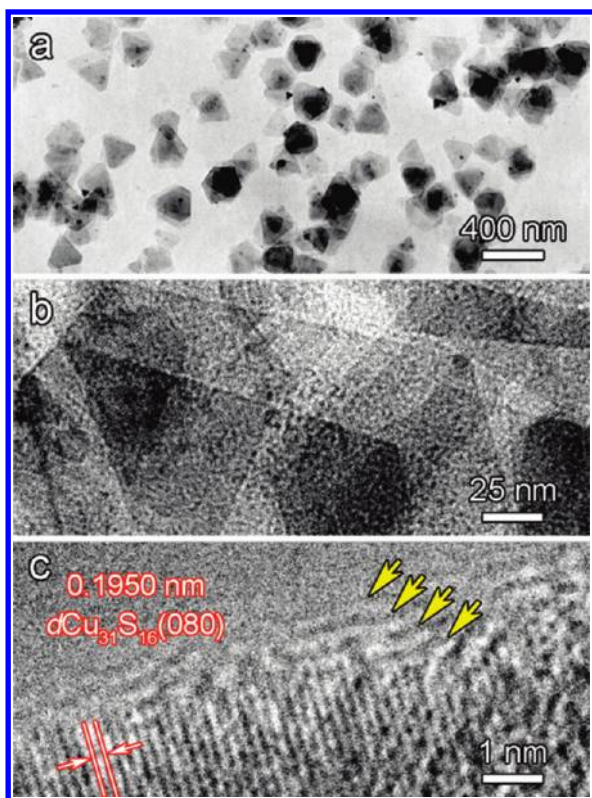


Figure 1. TEM image (a) and HRTEM images (b, c) of the resultant nanosheets obtained by a Cu to Sn ratio of 2:1. The identification of the crystalline plane is overlaid in panel c, while the yellow arrows indicate a step-like edge of a nanosheet.

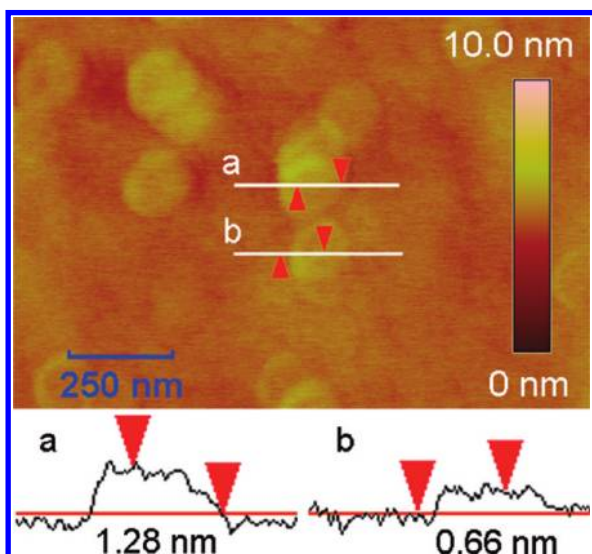


Figure 2. AFM image of the nanosheets obtained by a Cu to Sn ratio of 2:1 together with two height profiles recorded along the white lines overlaid.

brighter in color can still be identified, suggesting that the resultant nanosheets are very thin. Further interplanar distance analysis based on the HRTEM image (Figure 1c) suggests the resultant nanosheets are djurleite nanocrystals, while the crystal edge structure implies that the nanosheets are comprised of several atomic layers.

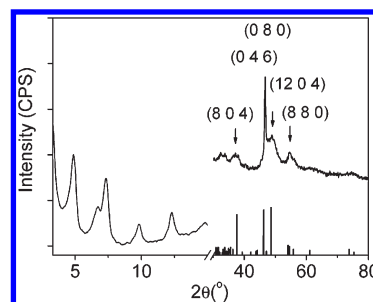


Figure 3. XRD pattern of nanosheets obtained by a Cu to Sn ratio of 2:1 together with the standard diffraction lines of bulk monoclinic djurleite (JCPDS card 23-0959) shown at bottom for comparison.

The thickness of the nanosheets shown in Figure 1 was further determined by AFM. The vertical resolution of the AFM used for current investigations can reach 0.3 Å by proper calibration. The upper panel of Figure 2 presents an overview image of several pieces of the nanosheets. The height profiles of selected nanosheets appearing to be single or overlapped are shown in the lower panel of Figure 2. The section analysis by averaging different measurements suggests that the thickness of a single layer nanosheet is about 6.6 Å and the thickness of two overlapped nanosheets is about 12.8 Å.

The atomic ratio of different elements in the resultant nanosheets was determined by both XPS and ICP-OES methods. The ratio of Sn:Cu:S was estimated to be 0.07:1.92:1.00 by XPS method. While by ICP-OES analysis, it was determined to be 0.097:2.01:1.00, quite consistent with the XPS results. Further analysis on Sn3d_{5/2} spectra, shown in Figure S1 in Supporting Information, suggests that Sn is doped into the crystal lattice of Cu₃₁S₁₆ nanosheets. But the Sn/Cu ratio in the resultant nanosheets is far below the feed ratio.

The crystalline structure of the nanosheets was analyzed by powder X-ray diffraction. The diffraction pattern between 40° and 80° (Figure 3) reveals that the nanosheets are of Cu₃₁S₁₆ (djurleite, Cu_{1.94}S, JCPDS card No. 23-0959; $a = 26.897$ Å, $b = 15.745$ Å, $c = 13.565$ Å, and $\beta = 90.13^\circ$).⁵³ Quite unexpectedly, in a low angle regime between 3° and 15°, a set of diffraction peaks appear, indicating that a periodical superstructure exists which is quite probably caused by the face-to-face stacking of the nanosheets as shown in Figure 1a. The periodic spacing was calculated to be 36.2 Å. As the length of a fully stretched alkyl chain of dodecanethiol is about 15.2 Å,⁵⁶ it can be deduced that thickness of the inorganic core of the nanosheets should be less than 1 nm.

Djurleite Nanoplates and Their Self-Assembled 1D Superstructure. The nanocrystals obtained by a Cu to Sn ratio of 8:1 are shown in Figure 4. Different from those shown in Figure 1a, the nanocrystals shown in Figure 4a appear as 1D nanorods at low magnification. However, the detailed structure shown by a higher magnification (Figure 4b) demonstrates that these rods are comprised of a large number of ultrathin triangular nanoplates assembled in a face-to-face manner, suggesting that increasing the Cu-to-Sn ratio dramatically decreases the size of the 2D nanosheets and meanwhile greatly increases the overlapping degree of the nanosheets, consequently leading to the formation of the rodlike 1D superstructure.

The composition of the nanoplates was also measured and the atomic ratio of Sn:Cu:S ratio was determined to be 0.030:1.98:1.00 according to the elemental analysis by XPS. It

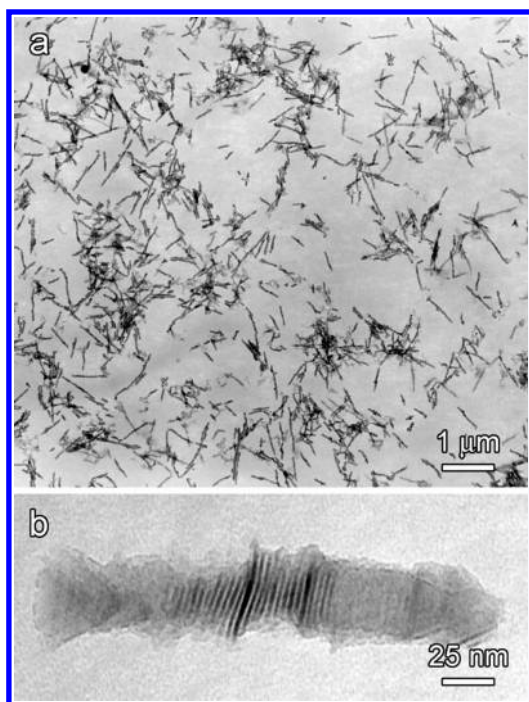


Figure 4. TEM images of 1D self-assembled nanorods made up of triangular nanoplates obtained by pyrolyzing $\text{Cu}(\text{acac})_2$ at 200 °C in dodecanethiol in the presence of SnCl_4 (Cu/Sn = 8:1) for 48 min.

is worth mentioning that the Sn/Cu ratio is further lowered in comparison with that in the djurleite nanosheets mentioned above.

The crystalline structure of this sample was also analyzed by XRD. The detailed results are shown in Figure S2 in Supporting Information. In general the nanoplates can also be indexed to the monoclinic djurleite phase. Quite similar to the djurleite nanosheets, the nanoplates also show a set of diffraction peaks in the small angle regime of 3–15°. The periodic spacing was calculated to be 35.8 Å, slightly smaller than that in the nanosheets.

DISCUSSION

As a matter of fact, the nanosheets comprised of a few atomic layers can be obtained with a top-down strategy by various types of exfoliation methods. But the resultant nanosheets are typically characterized by irregular shapes.^{6–9,14,15} Although the chemical synthesis based on bottom-up strategy is more favorable for obtaining regularly shaped nanomaterials including nanosheets and nanoplates,^{25,26} the nanosheets with a thickness of smaller than 1 nm are rare because on the one hand the nanocrystals of few-atomic-layer-thick are usually quite unstable;^{3,6,7} on the other hand, the size of the crystal nuclei may exceed 1 nm.⁵⁷

1. The Formation of Ultrathin Djurleite Nanosheets. The djurleite nanosheets shown in Figure 1 are characterized by their ultralow thickness of ~6.4–6.6 Å according the AFM measurements. In comparison with their 0D counterpart,⁵⁴ that is, $\text{Cu}_{31}\text{S}_{16}$ nanocrystals shown in Figure S3 in Supporting Information, the only difference with respect to the preparation is that the djurleite nanosheets were prepared in the presence of SnCl_4 . The process from the nucleation to the growth of 0D $\text{Cu}_{31}\text{S}_{16}$ nanocrystals formed by pyrolyzing $\text{Cu}(\text{acac})_2$ in dodecanethiol has previously been investigated.⁵⁴ It was demonstrated that the

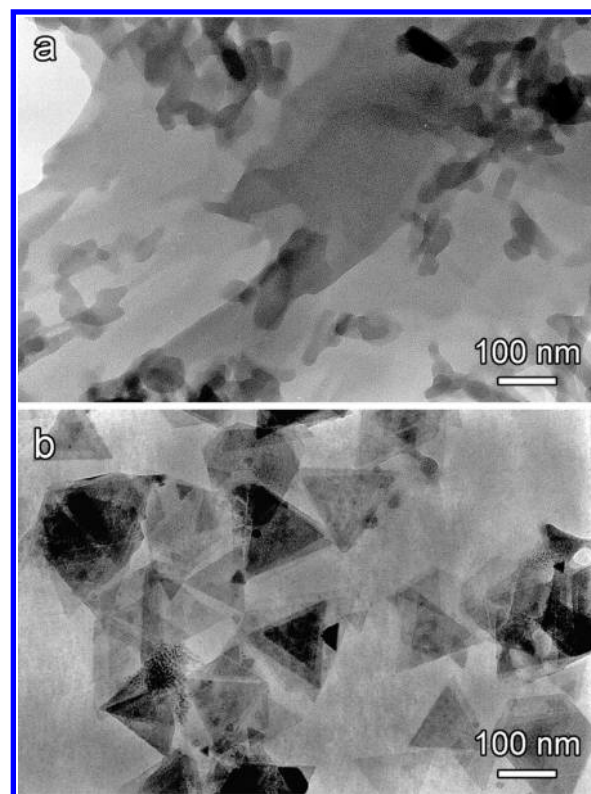


Figure 5. TEM images of I-sample 1 (a) and I-sample 2 (b).

uniformly sized $\text{Cu}_{31}\text{S}_{16}$ nanocrystals are generated at the cost of a lamellar structure formed by the copper and sulfur precursors.^{54,55} Similar lamellar structures are also found to be dominant in the sample extracted at 140 °C (I-sample 1) as presented in Figure 5a. In contrast, triangular nanosheets of larger than 100 nm appear in the sample obtained in 12 min at 200 °C (I-sample 2) as shown in Figure 5b, which implies that the nanosheets are born in the lamellar structures formed. These morphological differences are clearly reflected in their XRD patterns shown in Figure 6. In general, both of these two samples present similar successive diffraction peaks at low angle regime, suggesting that they both possess internal superstructures. However, apart from the appearance of monoclinic djurleite phase, I-sample 2 shows a d -spacing of 35.5 Å, larger than 33.9 Å for I-sample 1. But it remains slightly smaller than the d -spacing (36.2 Å) for the djurleite nanosheets eventually obtained at 200 °C in 48 min. Therefore, it is reasonable to conclude that the nanosheets are generated by consuming the lamellar structures formed by the $\text{Cu}(\text{acac})_2$ and dodecanethiol.

Nevertheless, it is still so far unclear how Sn leads to the formation of djurleite 2D nanosheets instead of 0D nanocrystals, meanwhile with only a very small amount is leftover in the finally obtained samples. To understand this phenomenon, XPS measurements were carried out to determine Sn in I-sample 1. It was quite unexpected that virtually no Sn signal was detected. According to previous literature reports, Sn, Cl, and ethanol can form a complex structure of $\text{Sn}_2\text{Cl}_6(\text{C}_2\text{H}_5\text{O})_2(\text{C}_2\text{H}_6\text{O})_2$;⁵⁸ therefore, Sn is quite possibly removed during the purification process by ethanol with dodecanethiol partly involved in forming certain complexes which are still unknown. To further provide experimental proofs on this speculation, two additional lamellar precursor samples were prepared. The first one, denoted as C-1

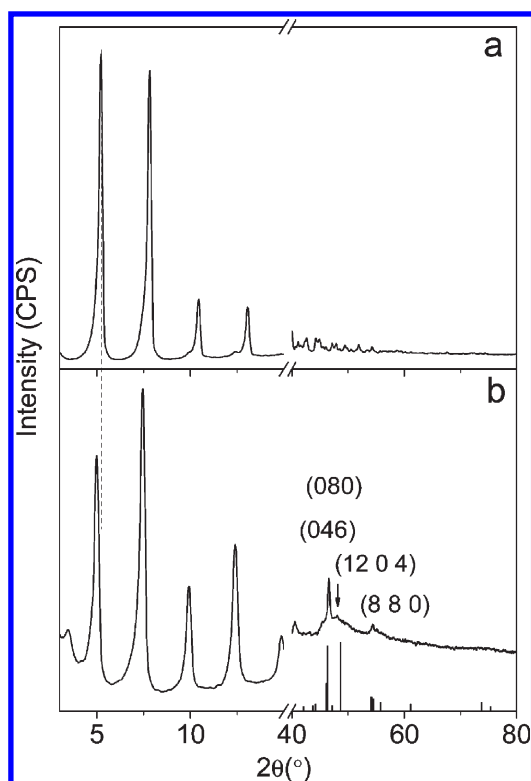


Figure 6. XRD patterns of I-sample 1 (a) and I-sample 2 (b) together with the line pattern of monoclinic djurleite (JCPDS card 23-0959) showing at bottom of frame b for comparison. A vertical dashed line is drawn across frames a and b to show the difference between the corresponding diffraction peaks from these two samples.

(control sample I), was prepared in the absence of Sn at 140 °C, while the second one (denoted as C-2) was prepared in exactly the same way as that for I-sample 1 except that the resultant sample was collected by centrifugation at 8000 rpm followed by blow drying with nitrogen stream. Then the *d*-spacing in the resultant samples were determined by XRD. The results are shown in Figure 7. According to the successive diffraction peaks appearing in the range of 3–15°, the *d*-spacing of the first sample (C-1) was calculated to be 35.7 Å, while that of the second sample (C-2) was of 35.1 Å, quite consistent with each other but larger than that of I-sample 1, that is, 33.9 Å. Therefore, it can be concluded that Sn is involved in the lamellar structure but can be removed by ethanol, which also explains why very much less Sn was leftover in comparison with the feed molar ratios of Sn to Cu with respect to both djurleite nanosheets (Figure 1) and nanoplates (Figure 4).

To know how Sn is involved in the lamellar structure, XPS measurements were performed on the above-mentioned two control samples, that is, C-1 and C-2. It was confirmed that there is only monovalent copper being present in both of these two samples, while in second control sample (C-2) Sn occurs in the tetravalent state. The atomic ratio of Cu:S:C in C-1 is of 1.07:1:11.66, quite close to 1:1:12, suggesting that Cu²⁺ was reduced to Cu⁺ and then forms a 1:1 complex with dodecanethiol. The atomic ratio of Cu:Sn:S:C in C-2 is of 0.94:0.06:1:12.7, suggesting that Cu is partly replaced by Sn by approximately 6.0%, forming a similar 1:1 complex with dodecanethiol. The absence of Sn in I-sample 1 suggests that Sn was extracted by ethanol during purification; consequently, I-sample 1

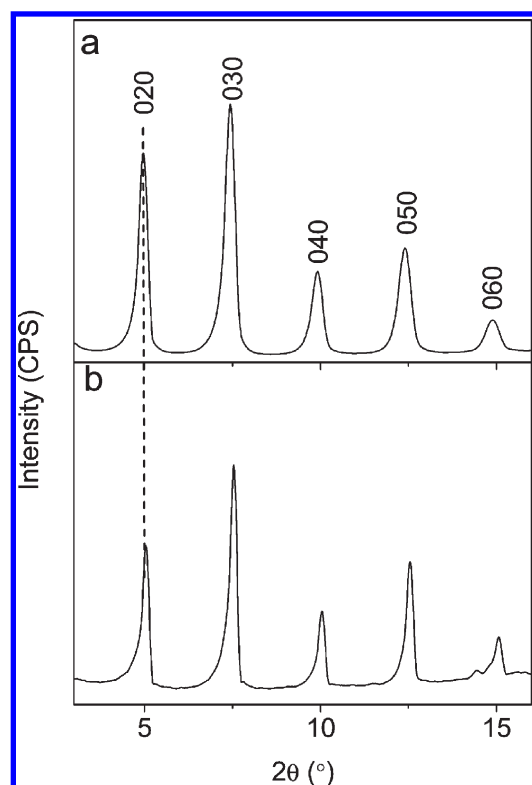


Figure 7. XRD patterns of C-1 (a) and C-2 (b) together with the reflection indexes. A vertical dashed line is drawn across panels a and b to show the difference between the corresponding diffraction peaks from these two samples.

presents a decreased thickness in comparison with C-2. In this context, it is reasonable to deduce that the Sn atoms binding on the surface of the nanosheets were extracted by ethanol during the purification. Thus, the *d*-spacing difference between the djurleite nanosheets (36.2 Å) and lamellar structures in C-2 (35.1 Å) becomes smaller than the thickness of the djurleite nanosheets (~6.5 Å) shown in Figure 1.

As a matter of fact, SnCl₄ and dodecanethiol can also form SnCl_{4-x}SR_x complexes.^{59–61} However, under the same preparative conditions for producing djurleite nanosheets no tin sulfide nanoparticles were generated in the reaction system of SnCl₄-in-dodecanethiol, suggesting that the SnCl_{4-x}SR_x complexes are very stable and can survive the whole preparation process. On the basis of all above-mentioned experiment proofs and observations, the formation mechanism of the ultrathin djurleite nanosheets is proposed as follows.

Before the thermal cleavage of the C–S bond above 140 °C, Cu, Sn, and dodecanethiol can form a lamellar structure in which Sn in tetravalent state partly replaces the monovalent copper without disturbing the huge lamellar skeleton constructed by monovalent copper and dodecanethiol. In such a supramolecular lamellar structure, Cu, Sn, and S form a central layer with alkyl chains serving protective layers on both sides. Upon the thermal decomposition of CuSR at further elevated temperature, the C–S bonds are broken to form the djurleite phase, while SnCl_{4-x}SR survives and remains capping on both sides of the resultant djurleite nanosheets and consequently prevents the nanosheets from further growing into 0D nanocrystals. In fact, Talapin and co-workers have recently demonstrated that molecular complex Sn₂S₆⁴⁻ can serve as a novel type of surface capping

ligands for a great number of colloidal nanocrystals and nanowires,⁶² which strongly support that the surface binding $\text{SnCl}_{4-x}\text{SR}_x$ complexes also act as surface ligands with respect to the current system. Nonetheless, $\text{SnCl}_{4-x}\text{SR}_x$ complexes can be removed by further forming complex structures with ethanol during the post-purification process. Therefore, a slight decrease in the thickness of the organic capping layer occurs. Consequently, the overall thickness increase caused by the formation of djurleite nanosheets of 6.5 Å is slightly compensated.

2. The Regular Shapes of the Djurleite Nanosheets. The second noticeable characteristic of the djurleite nanosheets is their regular shapes. As mentioned above, the nanosheets with a few atomic layers can easily be obtained but characterized by irregular shapes.^{6–9,63} In order to explain the regular shape of the current nanosheets, further TEM investigations were carried out. According to TEM results shown in Figure 1a, the djurleite nanosheets present three sorts of morphologies, that is, triangle, hexagon, and quasi-equilateral hexagon. The representatives of these three sorts of nanostructures are selected and presented in Figure 8. The SAED patterns of each nanosheet shown as insets demonstrated that they are single crystals. Further analysis on the SAED patterns suggests that the diffraction dots of 6-fold symmetry come from the (080) and (046) planes. Therefore, it can be concluded that (100) facet of djurleite phase forms the bottom and top surfaces of the nanosheets.

On the basis of the investigations of Evan on djurleite,⁵³ an atomic packing model that depicts the {100} facets of the monocline $\text{Cu}_{31}\text{S}_{16}$ is shown in Figure 9a. According to this model, $\text{Cu}_{31}\text{S}_{16}$ possesses a triangular packing of sulfur atoms from two groups of (046) planes and one group of (080) planes as highlighted by white lines overlaid, which can in principle interpret the formation of the regular shapes of the nanosheets shown in Figure 8. The crystal lattice of {100} facets of one piece of djurleite nanosheet is shown in Figure 9b. As indicated by the guide lines the (080) and (046) crystal planes can compose the representative shapes of nanosheets shown in Figure 8.

Djurleite $\text{Cu}_{31}\text{S}_{16}$ belongs to monoclinic crystal system which has only a 2-fold symmetry axis or symmetry plane. In principle, it is difficult to a form single crystal with a 6-fold symmetry axis. The interior angles overlaid on each nanosheet shown in Figure 8 demonstrate that both the triangles and hexagons are inequilateral, which further support that the nanosheets belong to monoclinic djurleite with the {100} facets being perpendicular to the normal direction, very consistent with the aforementioned analysis. The appearances of quasi-equilateral triangles and quasi-equilateral hexagons can be attributed to the fact that the β angle of monoclinic djurleite is 90.13° , quite close to 90° .

In general, nanocrystals growing under thermodynamically controlled growth conditions tend to form regular shapes enveloped by low-energy crystal facets. The formation of 2D nanocrystals involves two necessary conditions; that is, the growth along a certain axis is blocked and the growth along the reset two axes is promoted. The results shown in Figure 5b demonstrate that the initially formed nanosheets (12 min) are dominated by triangular ones with an average size of 131 ± 21 nm. In contrast, in the sample obtained in 48 min at 200°C , quite a percentage of hexagonal nanosheets appear apart from an increase in the average size (209 ± 33 nm), as shown in Figure 1a. Moreover, the quasi-triangular nanosheets presenting in the latter sample are also bigger than those shown in Figure 5b. Therefore, it can be deduced that the initially formed triangular nanosheets grow along lateral directions as the reaction goes on.

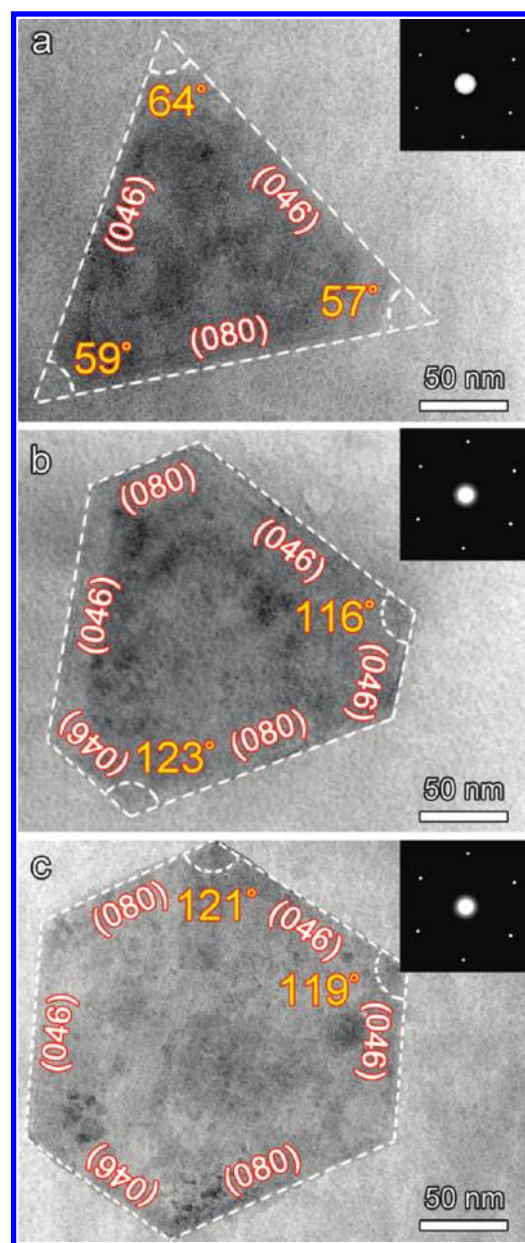


Figure 8. TEM images of three representative nanosheets obtained by a Cu to Sn ratio of 2:1 overlaid with identifications of the crystal planes for each edge and selected interior angles. Inset: SAED of the corresponding single nanosheets.

Because of the higher energy of three sharp angle tips, they gradually grow bigger and meanwhile change their shapes to more stable forms.

3. The Formation of 1D Superstructure Comprised of Djurleite Nanoplates. Note that SnCl_4 has a crucial impact on the morphology of djurleite nanocrystals, which find more proof from the following results obtained upon an increased feeding molar ratio of Cu/Sn. As mentioned in Results, apart from a decrease in the doping level of Sn, the resultant nanosheets are greatly reduced in size, leading to triangular nanoplates of ~ 36 nm as shown in Figure 4. The average d -spacing between two adjacent nanoplates is estimated to be around 3.4 nm based on TEM measurements on vertically arranged pieces shown in Figure 4b.

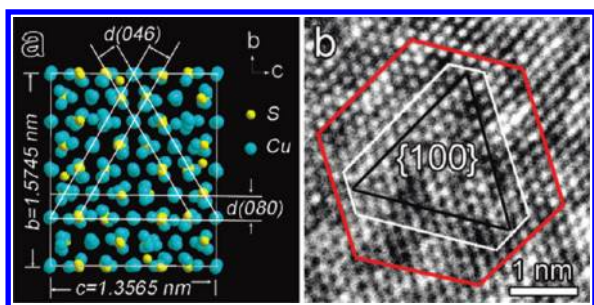


Figure 9. (a) Crystallographic model of the monoclinic djurleite structure viewed from the $[100]$ direction for depicting the arrangement of atoms of $\{100\}$ facets; (b) HRTEM image of one nanosheet obtained by a Cu to Sn ratio of 2:1 overlaid with imaginary shapes that may be formed according to the atomic arrangement of the atoms of $\{100\}$ facets.

It is worth mentioning that apart from the unique triangular shape, the 2D $\text{Cu}_{31}\text{S}_{16}$ nanoplates can self-assemble into 1D nanorods with an average length and width of 365 ± 145 nm and 36.0 ± 5.9 nm, respectively, as shown in Figure 4a, which is interesting but quite unexpected. As a matter of fact, the Co nanodiscs²⁷ and rare-earth oxide nanoplates^{28,29} were also found to have such a self-assembling tendency owing to the hydrophobic interaction offered by the surface capping agents possessing long alkyl chains. However, in addition to hydrophobic interaction, dipole interaction may also play an important role in the self-assembly of $\text{Cu}_{31}\text{S}_{16}$ nanoplates. According to previous reports, the dipole–dipole interaction among 0D Cu_2S nanocrystals is one of the key factors for them to form a 3D superlattice structure.^{17,18,64} Further, theoretical calculations confirm that the dipole direction of Cu_2S nanocrystal is parallel to the $[001]$ direction.⁶⁴ In fact, in coexisting djurleite ($\text{Cu}_{31}\text{S}_{16}$) and chalcocite (Cu_2S),⁶⁵ the typical orientation relationship between them is that $[010]$ or $[012]$ of $\text{Cu}_{31}\text{S}_{16}$ is parallel to $[010]$, and $[100]$ of $\text{Cu}_{31}\text{S}_{16}$ is parallel to $[001]$ of Cu_2S , which suggests that the dipole direction of $\text{Cu}_{31}\text{S}_{16}$ is parallel to $[100]$.⁶⁶ According to the growth mechanism discussed above, the bottom and top surface of the djurleite nanosheets belong to $\{100\}$ facets. It can be deduced that the bottom and top surface of the nanoplates with greatly reduced sizes should also belong to $\{100\}$ facets, which can find more support from their XRD pattern (Figure S2, Supporting Information) in which the diffraction of (804) plane, which is supposed to be the third strongest diffraction for bulk djurleite, is very weak. Therefore, it is reasonable to deduce that the dipole–dipole interaction plays an important role in the 1D self-assembled structures of the nanoplates. Although such a self-assembling behavior can also be observed from the face-to-face stacking of the regular nanosheets shown in Figure 1a, due to greatly reduced size the triangular nanoplates gain dramatically increased mobility partly due to their dispersibility in solution (Figure S4, Supporting Information); consequently they more readily form large-scale 1D self-assembled structures.

CONCLUSIONS

In summary, it was for the first time for us to demonstrate that SnCl_4 has a remarkable ability in regulating the shape of $\text{Cu}_{31}\text{S}_{16}$ nanocrystals formed by pyrolyzing $\text{Cu}(\text{acac})_2$ in dodecanethiol. Because SnCl_4 can coordinate with dodecanethiol forming stable complexes that subsequently serve as surface capping agents preferentially attached on the $\{100\}$ facets of the djurleite, the

ultrathin 2D djurleite nanocrystals doped with Sn were obtained. Owing to the dipole–dipole interactions along the $[100]$ direction and hydrophobic interactions offered by the surface capping dodecanethiol, the resultant nanosheets tend to stack face-to-face on each other, which becomes more evident with respect to much smaller triangular djurleite nanoplates obtained upon a reduced Sn/Cu feeding ratio, resulting in interesting 1D self-assembled nanorods comprised of djurleite nanoplates.

ASSOCIATED CONTENT

Supporting Information. (1) XPS analysis of Sn in $\text{Cu}_{31}\text{S}_{16}$ nanosheets and lamellar structure with Sn being involved; (2) X-ray diffraction of the djurleite nanoplates; (3) TEM and XRD results on $\text{Cu}_{31}\text{S}_{16}$ nanocrystals; (4) UV–vis absorption spectra of the as-synthesized nanosheets and nanoplates dispersed in dichloromethane together with photographs of the resultant solutions. This material is available free of charge via the Internet at <http://pubs.acs.org>.

AUTHOR INFORMATION

Corresponding Author

*E-mail: gaomy@iccas.ac.cn. Fax: +86 10 8261 3214.

REFERENCES

- Seo, J. W.; Jun, Y. W.; Park, S. W.; Nah, H.; Moon, T.; Park, B.; Kim, J. G.; Kim, Y. J.; Cheon, J. *Angew. Chem., Int. Ed.* **2007**, *46*, 8828–8831.
- Shang, N. G.; Papakonstantinou, P.; McMullan, M.; Chu, M.; Stamboulis, A.; Potenza, A.; Dhesi, S. S.; Marchetto, H. *Adv. Funct. Mater.* **2008**, *18*, 3506–3514.
- Yoo, E.; Okata, T.; Akita, T.; Kohyama, M.; Nakamura, J.; Honma, I. *Nano Lett.* **2009**, *9*, 2255–2259.
- Zhang, H. T.; Wu, G.; Chen, X. H. *Langmuir* **2005**, *21*, 4281–4282.
- Li, F.; Bi, W. T.; Kong, T.; Qin, Q. H. *Crystallogr. Res. Technol.* **2009**, *44*, 729.
- Geim, A. K.; Novoselov, K. S. *Nat. Mater.* **2007**, *6*, 183–191.
- Novoselov, K. S.; Jiang, D.; Schedin, F.; Booth, T. J.; Khotkevich, V. V.; Morozov, S. V.; Geim, A. K. *Proc. Natl. Acad. Sci. U.S.A.* **2005**, *102*, 10451–10453.
- Teweldebrhan, D.; Goyal, V.; Balandin, A. A. *Nano Lett.* **2010**, *10*, 1209–1218.
- Gordon, R. A.; Yang, D.; Crozier, E. D.; Jiang, D. T.; Frindt, R. F. *Phys. Rev. B* **2002**, *65*, 125407–1–125407–8.
- Mu, R.; Tung, Y. S.; Ueda, A.; Henderson, D. O. *J. Phys. Chem.* **1996**, *100*, 19927–19932.
- Takagaki, A.; Tagusagawa, C.; Hayashi, S.; Hara, M.; Domen, K. *Energy Environ. Sci.* **2010**, *3*, 82–93.
- Horiuchi, S.; Gotou, T.; Fujiwara, M.; Asaka, T.; Yokosawa, T.; Matsui, Y. *Appl. Phys. Lett.* **2004**, *84*, 2403–2405.
- Viculis, L. M.; Mack, J. J.; Kaner, R. B. *Science* **2003**, *299*, 1361–1361.
- Ci, L.; Song, L.; Jin, C. H.; Jariwala, D.; Wu, D. X.; Li, Y. J.; Srivastava, A.; Wang, Z. F.; Storr, K.; Balicas, L.; Liu, F.; Ajayan, P. M. *Nat. Mater.* **2010**, *9*, 430–435.
- Lin, Y.; Williams, T. V.; Connell, J. W. *J. Phys. Chem. Lett.* **2010**, *1*, 277–283.
- Ghezelbash, A.; Korgel, B. A. *Langmuir* **2005**, *21*, 9451–9456.
- Larsen, T. H.; Sigman, M.; Ghezelbash, A.; Doty, R. C.; Korgel, B. A. *J. Am. Chem. Soc.* **2003**, *125*, 5638–5639.
- Sigman, M. B.; Ghezelbash, A.; Hanrath, T.; Saunders, A. E.; Lee, F.; Korgel, B. A. *J. Am. Chem. Soc.* **2003**, *125*, 16050–16057.

- (19) Chen, Y. B.; Chen, L.; Wu, L. M. *Inorg. Chem.* **2005**, *44*, 9817–9822.
- (20) Chen, J.; Wu, L. M.; Chen, L. *Inorg. Chem.* **2007**, *46*, 586–591.
- (21) Chen, Y. B.; Chen, L.; Wu, L. M. *Chem. -Eur. J.* **2008**, *14*, 11069–11075.
- (22) Alivisatos, A. P. *Science* **1996**, *271*, 933–937.
- (23) Peng, Z. A.; Peng, X. G. *J. Am. Chem. Soc.* **2002**, *124*, 3343–3353.
- (24) Tang, Z. Y.; Kotov, N. A.; Giersig, M. *Science* **2002**, *297*, 237–240.
- (25) Jun, Y. W.; Choi, J. S.; Cheon, J. *Angew. Chem., Int. Ed.* **2006**, *45*, 3414–3439.
- (26) Lu, W.; Ding, Y.; Chen, Y.; Wang, Z. L.; Fang, J. *J. Am. Chem. Soc.* **2005**, *127*, 10112–10116.
- (27) Puentes, V. F.; Zanchet, D.; Erdonmez, C. K.; Alivisatos, A. P. *J. Am. Chem. Soc.* **2002**, *124*, 12874–12880.
- (28) Cao, Y. C. *J. Am. Chem. Soc.* **2004**, *126*, 7456–7457.
- (29) Si, R.; Zhang, Y. W.; You, L. P.; Yan, C. H. *Angew. Chem., Int. Ed.* **2005**, *44*, 3256–3260.
- (30) Joo, J.; Na, H. B.; Yu, T.; Yu, J. H.; Kim, Y. W.; Wu, F. X.; Zhang, J. Z.; Hyeon, T. *J. Am. Chem. Soc.* **2003**, *125*, 11100–11105.
- (31) Choi, S. H.; An, K.; Kim, E. G.; Yu, J. H.; Kim, J. H.; Hyeon, T. *Adv. Funct. Mater.* **2009**, *19*, 1645–1549.
- (32) Xiong, Y. J.; Xie, Y.; Du, G. A.; Su, H. L. *Inorg. Chem.* **2002**, *41*, 2953–2959.
- (33) Steinhagen, C.; Panthani, M. G.; Akhavan, V.; Goodfellow, B.; Koo, B.; Korgel, B. A. *J. Am. Chem. Soc.* **2009**, *131*, 12554–12555.
- (34) Riha, S. C.; Parkinson, B. A.; Prieto, A. L. *J. Am. Chem. Soc.* **2009**, *131*, 12054–12055.
- (35) Guo, Q. J.; Hillhouse, H. W.; Agrawal, R. *J. Am. Chem. Soc.* **2009**, *131*, 11672–11673.
- (36) Han, W.; Gao, M. Y. *Cryst. Growth Des.* **2008**, *8*, 1023–1030.
- (37) Yao, Z. Y.; Zhu, X.; Wu, C. Z.; Zhang, X. J.; Xie, Y. *Cryst. Growth Des.* **2007**, *7*, 1256–1261.
- (38) Liu, Z. P.; Liang, J. B.; Xu, D.; Lu, J.; Qian, Y. T. *Chem. Commun.* **2004**, 2724–2725.
- (39) Choi, S. H.; Kim, E. G.; Hyeon, T. *J. Am. Chem. Soc.* **2006**, *128*, 2520–2521.
- (40) Panthani, M. G.; Akhavan, V.; Goodfellow, B.; Schmidtke, J. P.; Dunn, L.; Dodabalapur, A.; Barbara, P. F.; Korgel, B. A. *J. Am. Chem. Soc.* **2008**, *130*, 16770–16777.
- (41) Connor, S. T.; Hsu, C. M.; Weil, B. D.; Aloni, S.; Cui, Y. *J. Am. Chem. Soc.* **2009**, *131*, 4962–4966.
- (42) Lee, H.; Yoon, S. W.; Kim, E. J.; Park, J. *Nano Lett.* **2007**, *7*, 778–784.
- (43) Jiao, S. H.; Xu, L. F.; Jiang, K.; Xu, D. S. *Adv. Mater.* **2006**, *18*, 1174–1177.
- (44) Lei, Y. Q.; Song, S. Y.; Fan, W. Q.; Xing, Y.; Zhang, H. J. *J. Phys. Chem. C* **2009**, *113*, 1280–1285.
- (45) Martinson, A. B. F.; Elam, J. W.; Pellin, M. J. *J. Appl. Phys. Lett.* **2009**, *94*, 123107–1–123107–3.
- (46) Sakamoto, T.; Sunamura, H.; Kawaura, H.; Hasegawa, T.; Nakayama, T.; Aono, M. *Appl. Phys. Lett.* **2003**, *82*, 3032–3034.
- (47) Li, Z. Q.; Yang, H.; Ding, Y.; Xiong, Y. J.; Xie, Y. *Dalton T.* **2006**, 149–151.
- (48) Gorai, S.; Ganguli, D.; Chaudhuri, S. *Cryst. Growth Des.* **2005**, *5*, 875–877.
- (49) Lim, W. P.; Wong, C. T.; Ang, S. L.; Low, H. Y.; Chin, W. S. *Chem. Mater.* **2006**, *18*, 6170–6177.
- (50) Zhang, P.; Gao, L. *J. Mater. Chem.* **2003**, *13*, 2007–2010.
- (51) Li, B. X.; Xie, Y.; Xue, Y. *J. Phys. Chem. C* **2007**, *111*, 12181–12187.
- (52) Lu, Q.; Gao, F.; Zhao, D. *Nano Lett.* **2002**, *2*, 725–728.
- (53) Howard, T.; Evans, J. *Science* **1979**, *203*, 356–358.
- (54) Han, W.; Yi, L.; Zhao, N.; Tang, A.; Gao, M.; Tang, Z. *J. Am. Chem. Soc.* **2008**, *130*, 13152–13161.
- (55) Yi, L.; Tang, A.; Niu, M.; Han, W.; Hou, Y.; Gao, M. *CrystEngComm* **2010**, *12*, 4124–4130.
- (56) Pileni, M. P. *J. Phys. Chem. B* **2001**, *105*, 3358–3371.
- (57) Mott, D.; Yin, J.; Engelhard, M.; Loukrakpam, R.; Chang, P.; Miller, G.; Bae, I. T.; Das, N. C.; Wang, C. M.; Luo, J.; Zhong, C. *J. Chem. Mater.* **2010**, *22*, 261–271.
- (58) Genge, A. R. J.; Levason, W.; Reid, G. *Acta Crystallogr. C* **1996**, *52*, 1666–1668.
- (59) Nelson, J. H.; Wilson, W. L.; Cary, L. W.; Alcock, N. W.; Clase, H. J.; Jas, G. S.; Ramsey-Tassin, L.; Kenney, J. W. *Inorg. Chem.* **1996**, *35*, 883–892.
- (60) Cunningham, D.; Mcginley, J. *J. Chem. Soc., Dalton Trans.* **1992**, 1387–1391.
- (61) Patel, K. S.; Shrivash, K.; Sharma, P. C.; Pandey, M.; Hoffmann, P. *Anal. Lett.* **2004**, *37*, 1953–1963.
- (62) Kovalenko, M. V.; Scheele, M.; Talapin, D. V. *Science* **2009**, *324*, 1417–1420.
- (63) Tang, Z. Y.; Zhang, Z. L.; Wang, Y.; Glotzer, S. C.; Kotov, N. A. *Science* **2006**, *314*, 274–278.
- (64) Zhuang, Z. B.; Peng, Q.; Zhang, B.; Li, Y. D. *J. Am. Chem. Soc.* **2008**, *130*, 10482–10483.
- (65) Buerger, M. J.; Wuensch, B. J. *Science* **1963**, *141*, 276–277.
- (66) Posfai, M.; Buseck, P. R. *Am. Mineral.* **1994**, *79*, 308–315.